Available online at www.sciencedirect.com
SCIENCE DIRECT®
Surface and Coatings Technology 177–178 (2004) 525–531
SURFACE & COATINGS TECHNOLOGY
www.elsevier.com/locate/surfcoat

Evaluation of microstructures and mechanical properties of chromized steels with different carbon contents

Jyh-Wei Lee*, Jenq-Gong Duh

Department of Materials Science and Engineering, National Tsing Hua University, Hsinchu, Taiwan, ROC

Abstract

Chromization process is a method for developing a surface coating providing hardness, wear and corrosion resistance. Three carbon steels, AISI 1020, 1045 and 1095 with 0.20, 0.45 and 1.0 wt.% carbon contents, respectively, were chromized with pack cementation process at 950 °C for 1, 4 and 9 h. The primary phase on the chromized surface is $(Cr,Fe)_2N_{1-x}$ and the rest is $(Cr,Fe)_{23}C_6$ phase. The thickness of the chromized layer obeys the parabolic rate law: $X=K\sqrt{t}$ and increases with chromization time and carbon contents in the matrix. The parabolic rate constants K are evaluated to be 4.04, 7.25 and 8.43 $\mu m/\sqrt{h}$ for AISI 1020, 1045 and 1095, respectively. The nanohardness of the chromized layer is 18 GPa, which is attributed to the $(Cr,Fe)_2N_{1-x}$ phase on the surface. Values of lower and upper critical loads of the chromized AISI 1020 steel decrease with increasing chromization time, whereas the increasing critical loads with chromizing time are observed on the chromized AISI 1045 and 1095 steels. High critical loads and sufficient adhesion properties are achieved due to the thicker $(Cr,Fe)_2N_{1-x}$ phase on the chromized surface.

Keywords: Chromization process; Chromized layer; Nanohardness; Scratch test; Critical load

1. Introduction

Surface modification process is a technique to deposit a foreign material onto the surface of interest to improve desired properties, such as wear, corrosion and high temperature oxidation resistance. Chromization process is one of the surface modification techniques that has been used for years. Chromization processes can be carried out by pack [1–14], salt bath [15], fluidized bed [16] and chemical vapor deposition [17] methods. Chromization is usually divided into two categories: soft chromization and hard chromization [2]. The former is employed on the alloys with less than 0.1 wt.% carbon to improve their corrosion and high temperature oxidation properties. Whereas, the hard chromization process is applied to the alloys with higher than 0.3 wt.% carbon to achieve a high hardness surface layer. Efforts to the soft chromization of alloys for high temperature corrosion purpose were reported [2–5,9,11,12]. Layer of chromium-rich phases were observed and could be further oxidized to form chromium oxides with excellent corrosion and oxidation resistances. Hard chromium carbide layers were revealed for the hard chromization process to achieve improved mechanical properties. For example, higher hardness [2,5,13,14,16,18] and good adhesion properties [18] were obtained in the chromized alloys. However, detailed mechanical property evaluations of hard chromization on alloys have never been studied in literature. Nor have any suitable chromization parameters for tribological application been investigated. The objective of this study was to evaluate the influence of carbon contents to mechanical properties of steels after hard chromization. Nanoindentation and scratch were conducted to explore the nanohardness and adhesion properties of chromizing coatings in different carbon containing steels. Microstructures and chemical analysis of chromized layers were also investigated.

2. Experimental procedures

Three commercial fully-annealed AISI 1020, 1045 and 1095 carbon steel plates were selected as starting materials. Specimens with $20\times20\times5$ mm^3 dimensions

*Corresponding author. Department of Mechanical Engineering, Tung Nan Institute of Technology, #152, Sec. 3, Pei-Shen Road, Shen-Ken, Taipei, 222 Taiwan, ROC. Fax: +886-2-86625919.
E-mail address: jefflee@mail.me.tnit.edu.tw (J.-W. Lee).

0257-8972/04/$ - see front matter © 2003 Elsevier B.V. All rights reserved.
doi:10.1016/j.surfcoat.2003.08.031

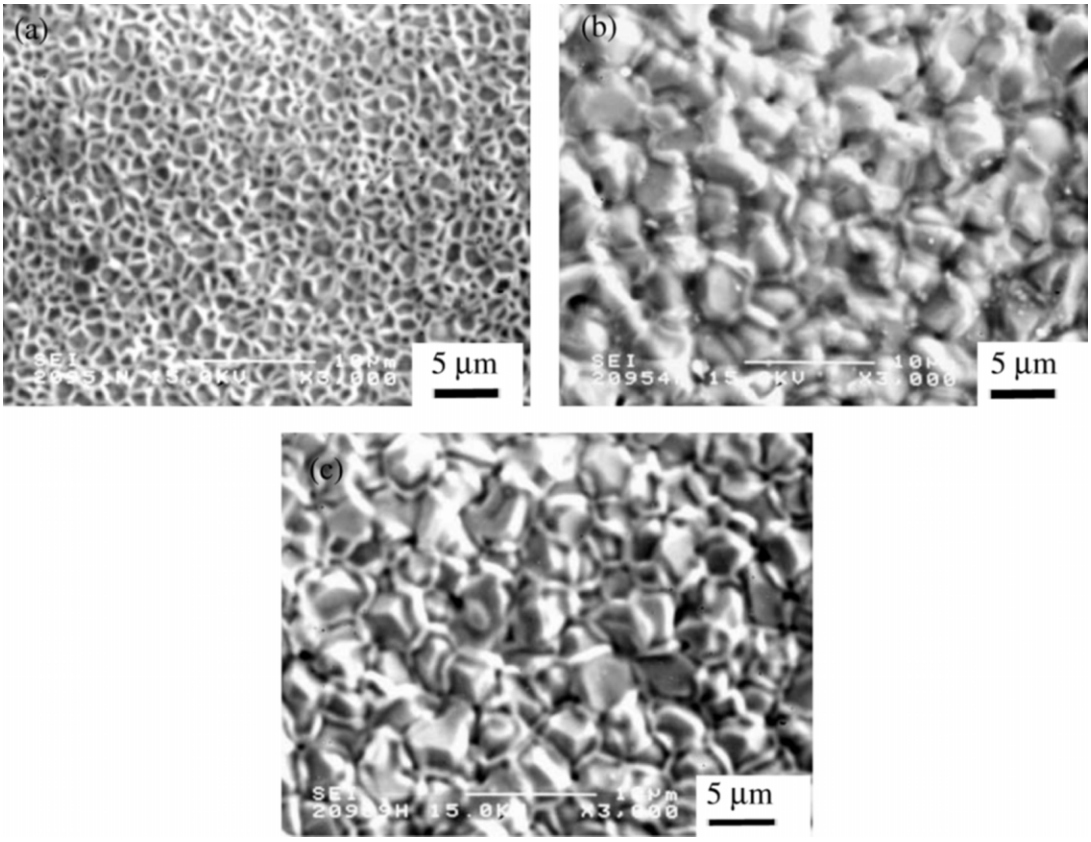

Fig. 1. Surface morphologies of AISI 1020 specimens chromized at 950 °C for (a) 1 h; (b) 4 h and (c) 9 h.

were cut from the carbon steel plate, abraded and polished up to 1 μm Al_2O_3 powder, washed in distilled water, ultrasonically degreased in acetone and rinsed in alcohol. Detailed pack cementation process was reported elsewhere [14]. The pack chromizations were performed at 950 °C for 1, 4 and 9 h, respectively. The powder mixture for chromizing contained 30 wt.% ferrochromium powder (71 wt.% Cr–0.03 wt.% C and balanced Fe), 2.5 wt.% ammonium chloride activator and 67.5 wt.% filler (alumina powder). Argon protection was employed to prevent oxidation of chromium.

Phases of the chromized specimens were identified with an X-ray diffractometer (Rigaku, Model DMAX-B) equipped with Cu target and graphite single crystal monochromater. The working condition was 40 kV and 100 mA.

Surface morphologies of chromized specimens were examined with a scanning electron microscope. The thickness of the chromized layers in different time intervals was also measured. The elemental redistribution of specimens after chromizing was detected with an Electron Probe Microanalyzer (EPMA, JEOL JXA-8800M) by quantitative analysis of concentration for Fe, Cr, C and N with the aid of ZAF-corrected program. The X-ray mapping technique was also employed to investigate the two-dimensional distribution of constituent elements.

Values of nanohardness of chromized coatings were investigated by means of a nanoindenter (Triboscope E, Hysitron, USA) equipped with a Berkovich 142.3° diamond probe tip, 3-sided pyramidal indenter. A 3000-μN load was chosen in the tests.

A scratch tester (REVETEST, CSEM, Switzerland) was used to carry out the scratch adhesion test. Acoustic emission signal and friction force were measured during the test. The adhesion strength is usually determined by the following terms: L_{C1} and L_{C2} [19]. L_{C1}, the lower critical load, was defined as the load where first cracks occurred (cohesive failure). L_{C2}, the upper critical load, was defined as the load where the first delaminations at the edge of the scratch track occurred (adhesion failure). Three scratch tracks were tested for each specimen with ramping loads up to 80 N.

3. Results and discussion

3.1. Microstructures of chromized layers

Surface morphologies of AISI 1020 specimens chromized at 950 °C for 1, 4 and 9 h, respectively, are shown

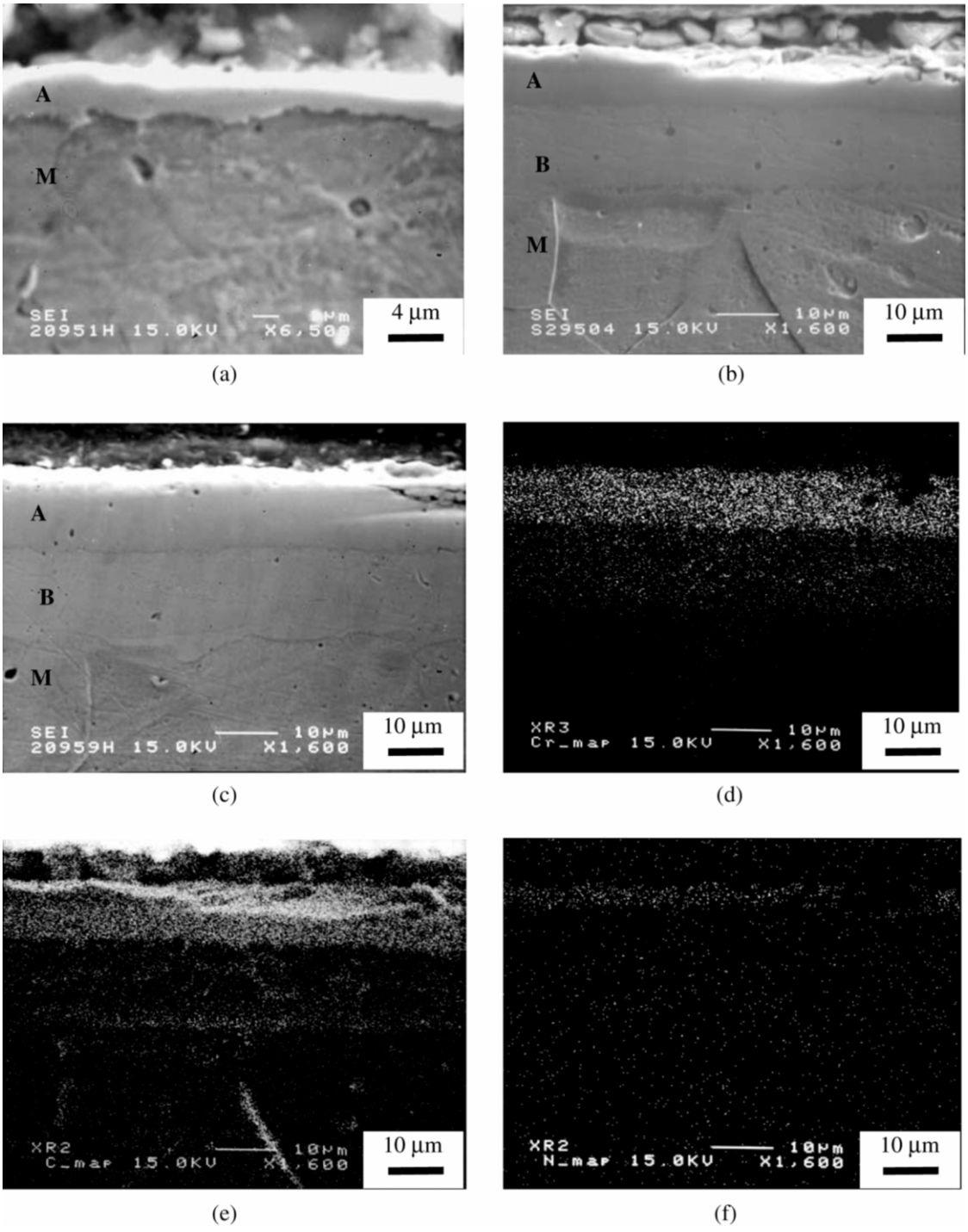

Fig. 2. Cross-sectional morphologies of AISI 1020 specimens chromized at 950 °C for (a) 1 h; (b) 4 h; (c) 9 h and X-ray mappings of (d) Cr; (e) C; and (f) N in Fig. (b). (Marker A, Chromized layer; B, chromization induced ferrite layer; M, steel matrix).

in Fig. 1a–c. The network-like surface structure is observed for the specimen chromized for 1 h in Fig. 1a. Granular structures with obvious grain boundaries are revealed on surfaces after chromized for 4 and 9 h in Fig. 1b and c. Specimens of AISI 1045 and 1095 steels chromized at 950 °C for 1, 4 and 9 h, respectively, all exhibit similar surface morphologies. Fig. 2 reveals, cross-sectional morphologies of AISI 1020 specimens chromized at 950 °C for various time. For the specimen chromized for 1 h, only a thin and wavy-like chromized layer, denoted as A, is found on the surface. However, for specimens chromized for 4 and 9 h, layers of

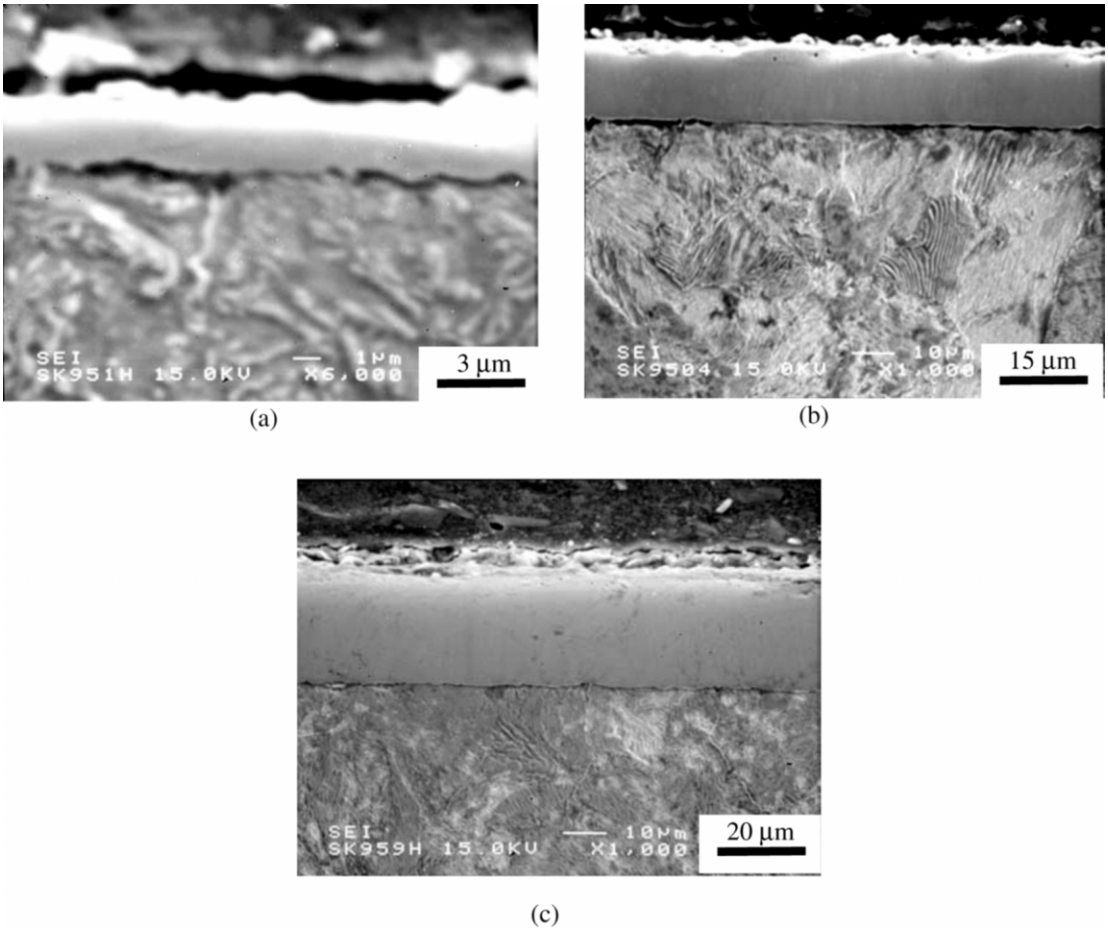

Fig. 3. Cross-sectional morphologies of AISI 1095 specimens chromized at 950 °C for (a) 1 h; (b) 4 h and (c) 9 h.

chromization-induced ferrite phase, denoted as B, are observed between chromized surface layers A and matrices M. The thickness of surface chromized layers increases with time. But chromium and carbon are enriched in the surface carbide layer A, chromized for 4 h, as shown in Fig. 2d and e. A small amount of nitrogen, as shown in Fig. 2f is also concentrated on the top of the chromized layer. In region B, the concentration of chromium is still higher than that in the matrix M as observed in Fig. 2d, which is attributed to the inward diffusion of chromium during chromization process. A chromization-induced ferrite layer was produced by the consumption of carbon in the matrix, while chromium carbide layer formed on the surface. A similar phenomenon of forming chromization-induced ferrite layer was also observed in the chromized dual phase Fe–Mn–Al alloy [14].

Cross-sectional morphologies of AISI 1095 specimens chromized at 950 °C for various time are shown in Fig. 3. Only chromized surface layers are found on the top of laminar pearlite matrices, yet no chromization-induced phase is found. The thickness of surface chromized layer also increases with time. Cross-sectional morphologies of chromized AISI 1045 specimens show the same appearance as AISI 1095. Thicknesses of surface chromized layers for three steels are calculated and listed in Table 1. Plots of thickness X (μm) vs. square root of chromizing time t (h) for three steels, reveals the parabolic rate law.

$$X = k\sqrt{t}$$

where X is the thickness; k is the rate constant.

For specimens AISI 1020, 1045, 1095, the rate constants were estimated to be 4.04, 7.35 and 8.43 $\mu m/\sqrt{h}$.

Table 1
Coating layer thickness of AISI 1020, 1045 and 1095 steels chromized at 950 °C for various time

Thickness (μm)	Chromizing time (h)		
	1	4	9
AISI 1020	2.55±1.02	7.19±1.68	13.24±0.63
AISI 1045	3.78±1.75	15.72±0.29	22.59±0.40
AISI 1095	4.65±2.08	16.17±0.02	27.02±2.60

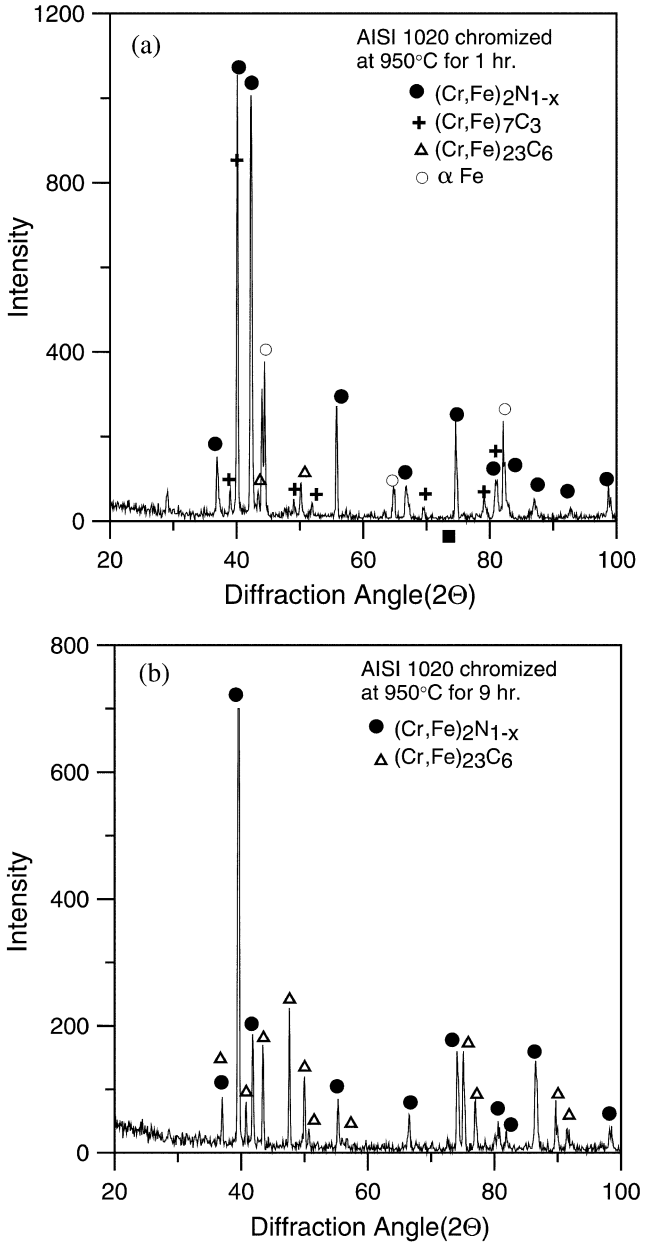

Fig. 4. X-ray diffraction pattern of the AISI 1020 specimen chromized at 950 °C for (a) 1 h and (b) 9 h.

The value of parabolic rate constants increases with carbon contents in the matrix, which means that the thickness of the chromized layer increases with carbon contents. Chen et al. reported a similar trend on the die steel with fluidized bed chromizing methods [16]. As compared to rate constants of AISI 1045 and 1095 steels, the rather low parabolic rate constant of AISI 1020 is owing to the limited content of carbon in the matrix. For dual Fe–Mn–Al alloy chromized at 1000 °C, the parabolic rate constant was calculated as 5.89 $\mu m/\sqrt{h}$ [14], which is about the same order in magnitude obtained in this study. The limited thickness of chromized layer in the dual phase Fe–Mn–Al–C alloy and AISI 1045 and 1095 steels is attributed to higher carbon contents in the matrix. The formation of chromium carbides retards the inward diffusion of chromium and thus restricts the thickness of chromized layer of higher carbon containing ferroalloy [1].

Table 2
Nanohardness of AISI 1020, 1045 and 1095 steels chromized at 950 °C for various time

Nanohardness (GPa)	Chromizing time (h)		
	1	4	9
AISI 1020	16.57±1.76	17.37±0.96	17.69±0.82
AISI 1045	17.71±0.69	18.08±0.82	18.06±1.04
AISI 1095	18.78±1.10	18.04±1.30	18.50±0.13

3.2. Phases and chemical analysis of the chromized layers

Structures of chromized layers for the AISI 1020 specimens chromized at 950 °C for 1 and 9 h were identified by X-ray diffractometry as shown in Fig. 4. The primary phase on the chromized surface is $(Cr,Fe)_2N_{1-x}$ and the rest is $(Cr,Fe)_{23}C_6$. Very little $(Cr,Fe)_7C_3$ phase can be found on the surface. The ferrite matrix is also revealed. The formation of $(Cr,Fe)_2N_{1-x}$ phase is caused by the nitridation reaction of chromium, iron and nitrogen from the decomposed NH_4Cl. For specimens chromized for 9 h as shown in Fig. 4b, the primary phase is still $(Cr,Fe)_2N_{1-x}$ and the rest $(Cr,Fe)_{23}C_6$ phase, whereas the $(Cr,Fe)_7C_3$ phase disappears and no ferrite phase is observed. On the basis of the X-ray diffraction analysis, the X-ray penetration depth of the chromized steel was estimated to be approximately 10 μm. As a result, the thicker chromized layer at 13.24 μm in the AISI 1020 specimen chromized at 950 °C for 9 h was thus sufficient to retard the X-

Table 3
Critical loads and failure modes of chromized AISI 1020, 1045 and 1095 steels by scratch tests

Critical load (N)		Chromizing time (h)		
		1	4	9
AISI 1020	L_{C1}[a]	54.7±0.6	43.8±3.8	22.7±2.2
	L_{C2}	66±4.6 (buckling)	50±2.6 (buckling)	43.8±0.9 (buckling)
AISI 1045	L_{C1}[a]	29.1±6.6	13.6±0.8	19.2±2.5
	L_{C2}	44.7±6.5 (buckling)	46.4±3.9 (buckling)	52.3±6.0 (buckling)
AISI 1095	L_{C1}[a]	29.9±4.0	25.7±1.5	30.7±2.6
	L_{C2}	43.0±6.4 (buckling)	52.3±1.0 (buckling)	69.0±0.3 (buckling)

[a] The failure mode in L_{C1} is conformal cracking.

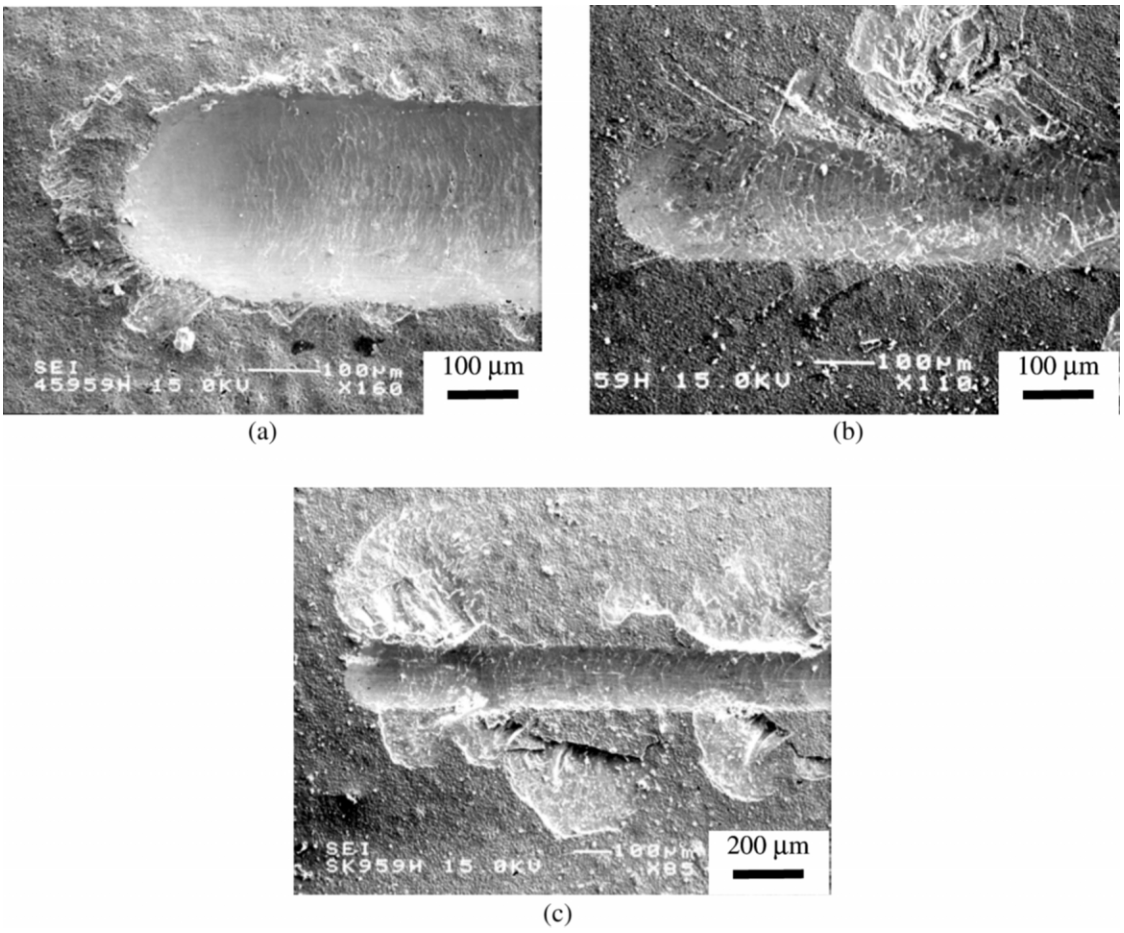

Fig. 5. Morphologies at the end of scratch tracks of (a) AISI 1020; (b) AISI 1045 and (c) AISI 1095 steels chromized at 950 °C for 9 h.

ray beam to detect the ferrite matrix beneath the chromized layer. On the contrary, the ferrite peaks were visible in the thinner chromized layer at 2.55 μm in the AISI 1020 specimen chromized at 950 °C for 1 h, as indicated in Fig. 4a. The X-ray diffraction patterns for AISI 1045 and 1095 specimens also reveal similar results. Arai [15] observed M_7C_3 phase when chromizing by salt bath at 1173 K from 30 to 72 000 s and $M_{23}C_6$ phase when chromized for longer than 3600 s.

The elemental redistribution of the AISI 1095 chromized at 950 °C for 9 h was detected by EPMA. High concentrations of chromium and carbon are observed near the outer surface. Concentration of nitrogen in the chromized layer reaches 11.29 atomic percent, which is responsible for the $(Cr,Fe)_2N_{1-x}$ phase. Based on the EPMA trace line of carbon, the thickness of carbide layer is 27 μm. The $(Cr,Fe)_{23}C_6$ phase is observed from the surface to 4-μm deep inside the coating layer, and is also present in the region ranging from 7 to 27 μm beneath the surface. In addition, the $(Cr,Fe)_7C_3$ phase is observed in the region ranging from 4 to 7 μm beneath the surface. Elemental redistributions of the AISI 1020, 1045 and 1095 specimens chromized at 950 °C for 1, 4 and 9 h all exhibit very similar appearance. However, the thickness of surface nitrogen-rich layer, i.e. the $(Cr,Fe)_2N_{1-x}$ phase, increases with carbon concentration and chromization time.

3.3. Nanohardness and scratch properties

The nanohardness data on the surfaces of the three steels chromized at 950 °C for 1–9 h are listed in Table 2. Nanohardness values of chromized AISI 1045 and 1095 steels in various time are almost equal to 18 GPa, whereas the chromized AISI 1020 steel is a little bit softer than that of chromized AISI 1045 and 1095 steels. Chen et al. measured the hardness of chromium carbide approximately 1600–1800 HV regardless the type of steel substrate [16]. In literature, the microhardness of $(Cr,Fe)_{23}C_6$ phases is 1200–1400 HV, and 2000–2500 HV for $(Cr,Fe)_7C_3$ phase [2], whereas the hardness of $(Cr,Fe)_2N_{1-x}$ phase is still unknown. Limited thickness and not well distributed $(Cr,Fe)_2N_{1-x}$ phase on the surface of the AISI 1020 steel chromized for 1 h is responsible for the lower hardness, 16.57 GPa. Since the main phase on the chromized surface is

$(Cr,Fe)_2N_{1-x}$ phase based on Figs. 2 and 5, it is argued that the measured surface hardness are contributed from the $(Cr,Fe)_2N_{1-x}$ phases mainly, rather than $(Cr,Fe)_{23}C_6$ phases, due to the very limited penetration depth of nanoindentation. The nanohardness of the $(Cr,Fe)_2N_{1-x}$ phase on the chromized layer was found to be 18 GPa in this study.

Adhesion properties of chromized coatings on the three steels are evaluated by scratch tests. Values of the L_{C1}, the lower critical load, and the L_{C2}, the upper critical load are listed in Table 3. Failure modes under critical loads are also summarized. Values of lower and upper critical loads of the chromized AISI 1020 steel decrease with increasing chromization time, while an increasing trend is observed on the chromized AISI 1045 and 1095 steels. The thicker $(Cr,Fe)_2N_{1-x}$ phase with increasing chromizing time is the major reason for the higher critical loads. For all three chromized steels, the conformal cracking is observed in the scratch channel under the lower critical load, L_{C1}. The failure mode of 1020, 1045 and 1095 steels chromized for 1 h are all buckling failures when the first delaminations at the edge of scratch tracks occur under the upper critical loads, L_{C2}. However, the failure mode under L_{C2} load differs when three steels chromized for longer time. Chipping failures are found on the AISI 1045 and 1095 steels chromized for 4 and 9 h, and also on the AISI 1020 steel chromized for 9 h. Morphologies of the ends for scratch channels of the AISI 1020 and 1045 steels chromized for 9 h are shown in Fig. 5a and b. For the chromized AISI 1020 sample, the cohesive failure mechanism of the coating appears to be conformal cracking in the scratch track. The adhesive failure is, however, caused by small amount of chippings near the end of the scratch track. For the chromized AISI 1045 samples, the cohesive failure mechanism of the coating attributes to the conformal and tensile cracking in the scratch track. The adhesive failure is also observed by the chipping near the end of scratch track. However, for the AISI 1095 specimens chromized at 950 °C for 9 h, more severe chipping failures are revealed in the scratch channel as shown in Fig. 5c. Chipping failures of AISI 1020, 1045 and 1095 samples chromized for 9 h occur due to the less sufficient adhesion properties between $(Cr,Fe)_2N_{1-x}$ and $(Cr,Fe)_{23}C_6$ layers.

4. Conclusions

1. Three carbon steels including AISI 1020, 1045 and 1095 have been chromized at 950 °C for 1, 4 and 9 h, respectively. The primary phase on the chromized surface is $(Cr,Fe)_2N_{1-x}$ and the rest is $(Cr,Fe)_{23}C_6$ phase. The thickness of chromized layer obeys the parabolic rate law and increases with chromization time and carbon contents in the matrix.
2. The nanohardness of the $(Cr,Fe)_2N_{1-x}$ phase on the chromized layer is 18 GPa measured by a nanoindenter under 3000 μN load.
3. Values of lower and upper critical loads of the chromized AISI 1020 steel decrease with increasing chromization time, while the increasing critical loads with chromizing time are observed on the chromized AISI 1045 and 1095 steels. Higher critical loads are obtained due to the thicker $(Cr,Fe)_2N_{1-x}$ phase on the chromized surface.

Acknowledgments

The authors gratefully acknowledge the financial support by the National Science Council, Taiwan, under Contract NSC-90-2218-E-236-003 and NSC-92-2216-E-236-001.

References

[1] G.H. Meier, C. Cheng, R.A. Perkins, W.T. Bakker, Surf. Coat. Technol. 39/40 (1989) 53.
[2] R.C. Jongbloed, Mater. Sci. Forum 163–165 (1994) 611.
[3] D.M. Miller, S.C. Kung, S.D. Scarberry, R.A. Rapp, Oxid. Met. 29 (3/4) (1988) 239.
[4] C.H. Koo, T.H. Yu, Surf. Coat. Technol. 126 (2000) 171.
[5] C.T. Liu, J.D. Wu, Surf. Coat. Technol. 43 (1990) 493.
[6] E. Godlewska, K. Godlewski, Oxid. Met. 22 (3/4) (1984) 117.
[7] S.C. Kung, R.A. Rapp, Oxid. Met. 32 (1/2) (1989) 89.
[8] W. Da Costa, B. Glesson, D.J. Young, Surf. Coat. Technol. 88 (1996) 165.
[9] D. Wang, Surf. Coat. Technol. 36 (1988) 49.
[10] N.H. Heo, M.T. Kim, J.H. Shin, C.Y. Kim, Surf. Coat. Technol. 124 (2000) 39.
[11] H.L. Du, J. Kipkemoi, D.N. Tsipas, P.K. Datta, Surf. Coat. Technol. 86–87 (1996) 1.
[12] S. Besenicar, N.W.J. Haanappel, V.A.C. Haanappel, T. Fransen, P.J. Gellings, Mater. High Temp. 9 (4) (1991) 193.
[13] F.S. Chen, K.L. Wang, Surf. Coat. Technol. 115 (1999) 239.
[14] J.W. Lee, J.G. Duh, S.Y. Tsai, Surf. Coat. Technol. 153 (2002) 59.
[15] T. Arai, S. Moriyama, Thin Solid Films 259 (1995) 174.
[16] F.S. Chen, P.Y. Lee, M.C. Yeh, Mater. Chem. Phys. 53 (1998) 19.
[17] A.J. Perry, Wear 67 (1981) 381.
[18] J.W. Lee, J.G. Duh, in: A. Kumar, Y.W. Chung, J.J. Moore, G.L. Doll, K. Yatsui, D.S. Misra (Eds.), Surface Engineering: Science and Technology II, first ed., TMS, Warrendale, 2002, p. 283.
[19] W. Heinke, A. Leyland, A. Matthews, G. Berg, C. Friedrich, E. Broszeit, Thin Solid Films 270 (1995) 431.